Available online at www.ijournalse.org

Emerging Science Journal

Vol. 4, Special Issue "IoT, IoV, and Blockchain", (2020, 2021)

Minimal Redundancy Linear Array and Uniform Linear Arrays Beamforming Applications in 5G Smart Devices

Satyanand Singh [a*]

[a] *Assistant Professor, School of Electrical and Electronics Engineering, Fiji National University, Suva, Fiji*

Abstract

Minimum Redundancy Linear Arrays (MRLAs) and Uniform Linear Arrays (ULAs) investigation conducted with the possibility of using them in future 5G smart devices. MRLAs are designed to minimize the number of sensor pairs with the same spatially correlated delay. It eliminates selected antennas from the entire composite antenna array and preserves all possible antenna spacing. MRLAs have attractive features for linear sparse arrays, even if the built-in surface is deformed, it works without problems. To our knowledge, MRLAs have not been applied to smart devices so far. In this work, a 7-element ULAs and 4-element MRLAs (same aperture) were used for the simulation. The Half Power Beamwidth (HPBW) is 0.666 and the Null-to-Null Beamwidth (BW_{NN}) is 1.385 in ψ-space. In comparison, the standard 4-element arrays are 1.429 and 3.1416, while the standard 7-element linear arrays are 0.801 and 1.795 respectively. Experimental results show that 4-element MLRAs have a narrower mean beam, much higher sidelobes and shallow nulls. Therefore, in terms of main lobe features, 4- elements MRLAs have an improvement over the standard 7-element ULAs.

Keywords:

Minimum Redundancy Linear Arrays;
MRLAs; Uniform linear arrays (ULAs);
Minimum Redundant Array (MRA);
Prolate Spheroidal Sequences (PSS);
Multi-Beam Antenna (MBA);
Planar Aperture Antennas (PAAs).

Article History:

Received:	15	June	2021
Revised:	04	September	2021
Accepted:	17	September	2021
Published:	06	October	2021

1- Introduction

Over the past two decades, the development of wireless communication systems has dramatically changed our way of life. Potential wireless support applications such as multimedia devices, the Internet of Things (IoT), and intelligent transportation systems require gigabit data rates per second that cannot be handled by current 4G communications systems due to limited bandwidth. An advanced mobile system is urgently needed to overcome bandwidth limitations. The International Telecommunication Union has licensed several millimeter-wave (mm-wave) spectrums. Potential fifth-generation (5G) and higher applications, including 24.25-27.5, 37-40, and 66-76 GHz [1]. Since then, millimeter-wave research has gained widespread attention.

MRLAs have many useful properties that have been studied primarily in the past in conjunction with radio astronomy. System belong to the class of linear sparse arrays, this is a subset of non-uniform linear arrays, and provide the maximum aperture for a given number of elements, or conversely, provide the minimum number of elements for a given aperture [2]. BouDaher et al. (2016) compared Direction of Arrival (DOA) estimation accuracy with three different non-uniform array geometries: minimum redundant array, nested array, common prime array, and mutual coupling of two antenna types that is, dipole antenna and microstrip antenna [3]. Jan Kui Chang et al. investigated and compared the results of using uniform, coprime, nested, MRA and a coprime array with displaced subarrays (CADiS) under the same physical sensor number, and the recommended array aperture for sparse and non-circular light sources have been greatly increased estimated accuracy [4].

* **CONTACT**: satyanand.singh@fnu.ac.fj

DOI: http://dx.doi.org/10.28991/esj-2021-SP1-05

© 2020 by the authors. Licensee ESJ, Italy. This is an open access article under the terms and conditions of the Creative Commons Attribution (CC-BY) license (https://creativecommons.org/licenses/by/4.0/).

To overcome high bandwidth loss and high gigabit data rates, 5G may use several promising technologies, including high gain array antennas and multi-beam antenna (MBA) communication systems [5, 6]. Recently Guo et al. investigated two new planar aperture antennas (PAAs) with high gain and high aperture efficiency of an open cavity, fed differentially on two parallel edges by a grounded coplanar waveguide [7], array antennas uses a broadband linearly polarized antenna elements with complementary sources [8], broadband microstrip array antennas with high antenna gain have been proposed for millimeter-wave applications [9]. Cheng et al. (2008) [10] and Chen et al. (2009), various MBAs were implemented based on reflective arrays, transmission lenses [11], and beamforming circuits [12]. The compact size combination of millimeter-wave antennas and multiple-input multiple-output technology has also been studied in base stations [13] and mobile terminals [14]. In addition, Wenyao Zhai et al. studied dual-band technology for multi-gigabit per second (Gbps) cellular applications for 5G communications and supports low-cost multi-layer technologies [15, 16].

Wonbin Hong et al. used mmWave 5G system benchmarks to study the effectiveness, existing limits, and required future research topics for mmWave 5G antenna design technologies [17]. For a given number of antennas, a linear array that achieves maximum resolution is advantageous for Earth's rotation aperture synthesis. This type of array is called a minimally redundant linear array. This is achieved by reducing the redundant space present in the array. Various methods are being considered to find the best array for a large number of antennas [17]. A systematic analysis of the regular patterns of these sequences shows that it is possible to generalize the best sequences. The best configuration can also be used to distribute workstations in a synthetic aperture array.

The ULA and the sparse linear array (SLA) were investigated and compared by Mohammad et al., and numerous advantages were discovered, including more degrees of freedom (DOF), higher resolution, and robustness against mutual coupling [18]. One of the applications encountered with uneven arrays is decimation or sparse array problems. In this case, start with a uniform linear array of TV elements or a linear aperture of length L. It has the required weight and associated beam pattern. Next, build a linear array with fewer elements and retain the desired beam pattern characteristics. In some cases, elements can be placed anywhere in the row. Otherwise, the positions are restricted to a uniform grid. The motivation is to reduce the cost and complexity of the array by reducing the number of sensors.

Antenna arrays and beamforming systems have become vital components of most modern wireless communication systems, and they play a critical role in delivering high capacity and data rates. Using beamforming techniques with antenna arrays, such as in multiple-input multiple-out (MIMO) mobile systems, radar, sonar, satellite, and many other recent applications, such as wireless sensors and medical networks, signals can be received more efficiently, and system performance can be greatly improved [19]. Millimeter-wave frequencies are used in fifth-generation (5G) mobile systems and networks beyond that, where wider bandwidths are available, to boost system capacity and deliver better data rates for consumers. However, because of substantial air propagation losses, millimeter-wave frequencies must be amplified using an efficient antenna array system [20]. One of the most essential capabilities of antenna arrays is the capacity to focus the radiation pattern in the desired directions while also controlling the level of undesirable radiations such as sidelobes, which collect unwanted interfering signals. As a result, one of the most essential needs for establishing a greater signal-to-interference ratio and spectral efficiency is to provide a high-gain mainlobe while minimizing sidelobe levels (SLLs). There is a variety of SLL reduction approaches in the literature, including simple constant tapering windows [21], optimized tapering windows [22], and a variety of additional effective optimization techniques [21].

The iterative SSL reduction is illustrated in Figure 1 by the flow chart, in which the initial conditions are set initially, and then the sidelobes are sequentially decreased one by one to reach the needed SLL.

This paper presents an iterative process for adjusting the loading levels to achieve the sidelobe level limitations in order to provide a universal and array configuration-independent SLL reduction technique with a quicker convergence time and adaptive beampattern creation. The pattern errors are computed and validated against the restrictions at each iteration. If a constraint is exceeded, the sector's loading is increased, and the weights are adjusted. The suggested algorithm begins by calculating the maximum SLL, then canceling it, determining the new weighted vector that results, and then moving on to the next greatest SLL, and so on. The technique is repeated until the SLL is satisfactory or the desired form of the radiation pattern is obtained. As with most optimization techniques, the proposed technique has adaptation and SLL control capabilities, but with a faster convergence time, the ability to work on any array configuration with inter-element spacing less than one wavelength in distance, and the ability to work effectively under mutual coupling. The number of iterations to discover the optimum weights is independent of the array size in the proposed iterative technique, and the processing time can be sped up by determining the best angle sampling step sizes.

The goal is to find weights that maximize the array's directivity while staying within a set of beam pattern constraints that keep sidelobe levels to a minimum. The method was created in the context of linear arrays of isotropic elements, but it can also be applied to non-isotropic elements and arrays of any shape.

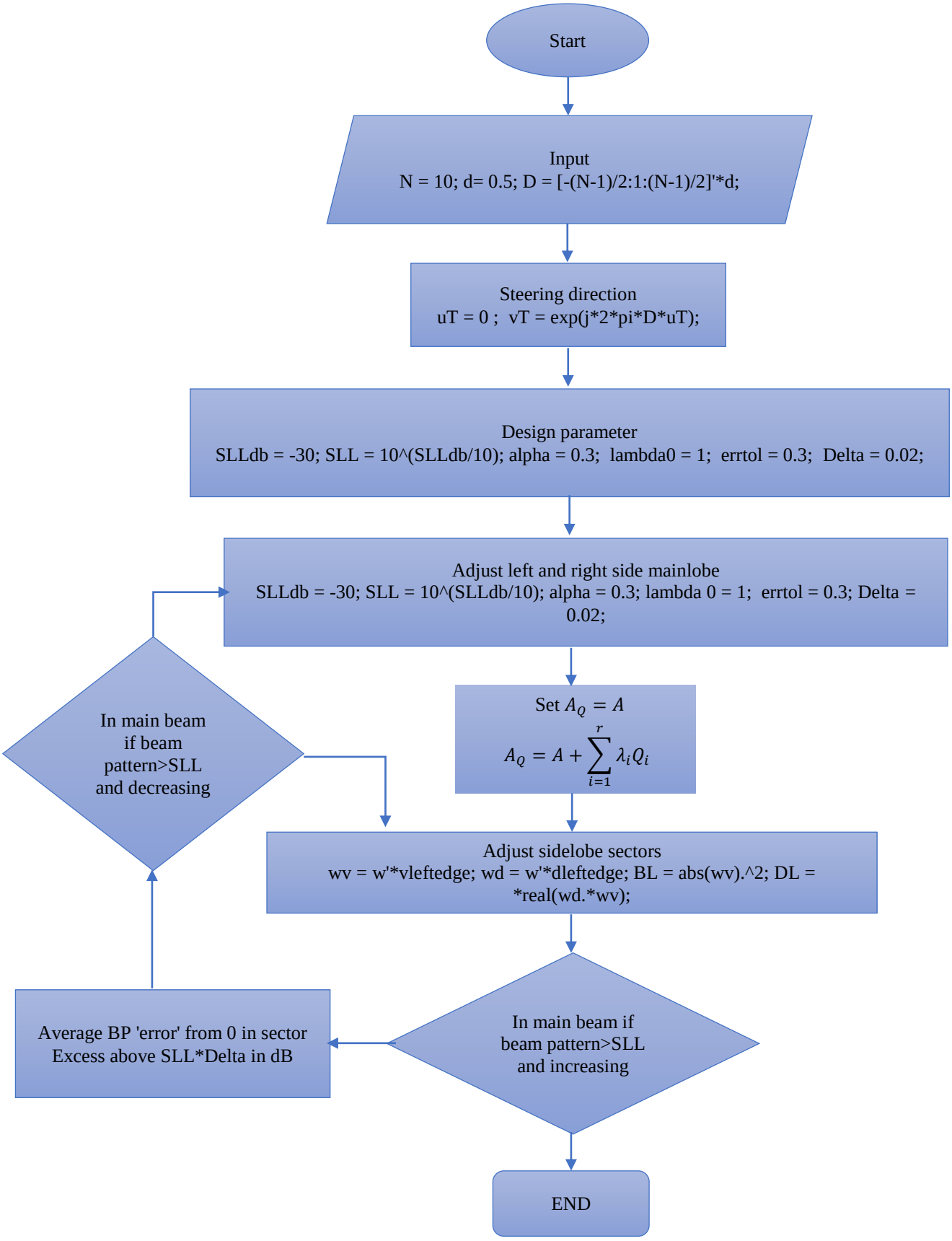

Figure 1. The iterative sidelobe level (SLL) reduction procedure is depicted as a flowchart.

2- Minimum Redundant Linear Arrays and Uniform Linear Arrays Model

This section describes the antenna array models by considering MRLAs and ULAs Model.

2-1- Minimum Redundant Linear Arrays (MRLAs) Application as Unevenly Spaced Linear Arrays

Consider a class of non-uniform linear arrays called MRLA. We limit our attention to build arrays on Grid structure with grid spacing 'd'. MRLAs are designed to minimize the number of sensor pairs with the same spatially correlated delay. Figure 2 shows an "ideal" MRLA. This is a 4-element array, which is equivalent to a standard linear array with a 7-element aperture. MLRA eliminates selected antennas from the entire composite antenna array and preserves all possible antenna spacing. Conventional or complete array with many antenna element combinations than can generates specified spatial lags d, 2d, 3d, 46, 5d, and 6d. Taking into account the numbers from 0 to 6, the antenna pairs {0, 1} generates a spatial lag of 1, {4, 6} generates a spatial lag of 2, {1, 4} generates a spatial lag of 3, {0, 4} generates a spatial lag of 4, {1, 6} generates a spatial lag of 5, and {0, 6} generates a spatial lag of 6 as represented in Table 1. MLRA carefully removes selected antenna elements so that fixed antenna elements can generate all gaps between zero and a specified maximum number. Like other sparse arrays, MLRA can identify more sources than sensors. However, its advantage is that it forms the largest co-array for a specified number of elements, provides the largest aperture in nested, co-primed, and hyper-nested arrays, and offers the highest resolution.

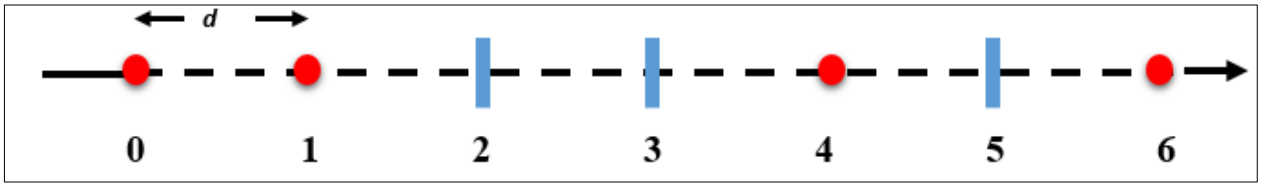

Figure 2. 4-element array equivalent to a standard linear array with a 7-element aperture of ideal MRLA.

MRLA configuration indicated in Figure 2 allows us to estimate at least one $(i-j)$ combination from 0 to 6:

$$E[x(t,id)x^*(t,jd)] \triangleq R_x\big((i-j)d\big) \quad (1)$$

Table 1. Sensors position at 0, 1, 4, 6 and its corresponding lag.

Position of the Sensors	Lag in terms of d
0-1	d
0-4	4d
0-6	6d
1-4	3d
1-6	5d
4-6	2d

Display the output of a 7-element standard linear sensor. When arranged in a 7×1 vector x(t), the correlation matrix becomes a 7×7 matrix as:

$$R_x = E[x(t)x^H(t)] \quad (2)$$

Therefore, use a 4-element array, a 7-element standard array with a correlation matrix of all elements are all of the form $R_x\big((i-j)d\big), i = 0,\dots,6; j = 0,\dots,6$. Many of the best processing algorithms are based on Rx. Therefore, the performance of a 4-element MRLA can be as good as a 7-element standard linear array. The length of the aperture is expressed as Na and measured by the number of grid intervals. Considering Na = 6 and N = 4 in the Figure 2.

To compute the number of times each spatially correlated delay is included in the array, we assume that the elements are evenly weighted, and then calculate the correlation of w with itself.

$$c(\gamma) \triangleq \sum_{|m-n|=\gamma} w_m w_m^* \quad (3)$$

The resulting function in Equation 3 is called a co-array and is a symmetric function. From the perspective of effective space, in sampling we want to set the co-array to unity instead of the origin. N_a indicates the maximum aperture size required in units of the element spacing d. The total aperture distance is given by N_a d. There are several MRLA configurations that provide the required aperture. If an array with this property is found then N_a can be computed as:

$$N_a = \frac{N(N-1)}{2} \quad (4)$$

This is the number of different off-diagonals of N × N correlation matrices Rx. Unfortunately, such an array (also called perfect array) $N > 4$ does not exist. For large arrays, consider two options. First, this option creates an array such that $c(\gamma)$ is zero or one (excluding the origin). These are called non-redundant arrays and are a representative set, as shown in Table 2.

Table 2. Non-redundant arrays and representative sets of sensors.

Number of Sensors	Position of Sensors and its Separation	D
2	. 1 .	1
3	. 1 . 2 .	1
4	. 1 . 3 . 2 .	1
5	. 1 . 3 . 5 . 2 .	1.10
6	. 1 . 3 . 6 . 2 . 5 .	1.13
7	. 1 . 3 . 6 . 8 . 5 . 2 .	1.19
8	. 1 . 3 . 5 . 6 . 7 . 10 . 2 .	1.21
9	. 1 . 4 . 7 . 13 . 2 . 8 . 6 . 3 .	1.22
10	. 1 . 5 . 4 . 13 . 3 . 8 . 7 . 12 . 2 .	1.22

Corresponding co-arrays with $N > 4$ have "gap" or "holes" in their value. The value D is the ratio of the Aperture length Na to the aperture length of the virtual complete array $(N(N-1)/2)$. Our aim is to construct gap-free sequences and the largest possible aperture. These are called minimal redundant arrays. Select the location of the sensor so that Na is as large as possible without gaps. The N_a can be expressed in terms of number of redundancies N_R and number of holes N_H as follows:

$$N_a = \frac{N(N-1)}{2} - N_R + N_H \quad (5)$$

Table 3. Minimum Redundancy Linear Arrays.

N	N_R	N_a	$\frac{N^2}{N_a}$	$\frac{N(N-1)}{2N_a}$	Arrays
3	0	3	3.0	1.0	12
4	0	6	2.67	1.1	132
5	1	9	2.78	1.11	1332 & 3411
6	2	13	2.77	1.15	13162 & 15322 & 11443
7	4	17	2.88	1.24	136232 & 114443 & 111554
8	5	23	2.78	1.22	1366232 & 1194332
9	7	29	2.79	1.24	136232 & 12377441 & 11(12)43332
10	9	36	2.78	1.25	1237441
11	12	43	2.81	1.28	1237441
12	16	50	2.88	1.32	1237441&111(20)5433
13	20	58	2.91	1.34	111(24)5433& 11671(10)3423143499995122
14	23	68	2.88	1.34	11671(10)3423& 11355(11)66611
15	26	79	2.85	1.33	11355(11)66611
16	30	90	2.84	1.33	11355(11)66611
17	35	101	2.86	1.35	11355(11)66611

Some authors have developed techniques to produce low redundancy Array. Pearson et al. develop effective and constructive procedure Optimal placement of the sensor [18]. Ruf uses simulated annealing to obtain low-redundant arrays and provides results for N <30 (Na <287) [19]. Linebarger et al. developed a boundary that provides an algorithm for constructing sparse arrays [20]. Linebarger provides a fast calculation method for arrays [21]. Table 3 represents all possible combination of MRLAs for $N = 3\ to\ 17$ and $N_a = 3\ to\ 101$.

2-2- Uniform Linear Arrays (ULAs)

Uniform Linear Array (ULA) is a collection of sensor elements distributed equidistantly along a straight line. The most common type of sensor is a dipole antenna that sends and receives airborne electromagnetic waves. On the z-axis there are seven elements with a uniform spacing equal to d. The origin has been placed at the center of array to indicate coordinate system. This centering brings computing benefits and is used throughout the simulation.

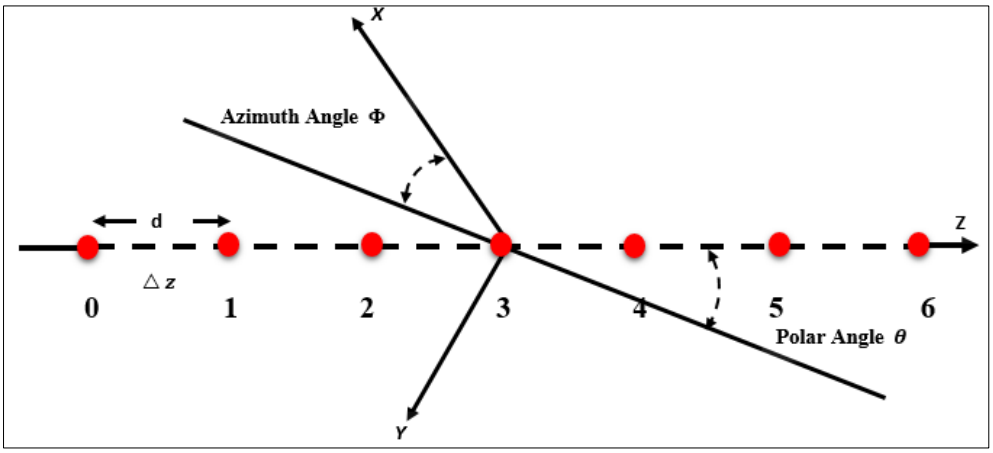

Figure 3. Uniform Linear Arrays of 7-elements located on the z-axis with uniform spacing "d".

Figure 3 illustrates ULAs of 7-elements located on the z-axis with uniform spacing "d". The mathematical position of the antenna array element is as follows:

$$p_{zn} = \left(n - \frac{N-1}{2}\right) d, \quad n = 0,1,2, \dots, N-1 \tag{6}$$

and;

$$p_{xn} = p_{yn} = 0 \tag{7}$$

The uniform antenna array manifold vector $v_k(K)$ can be calculated by substituting Equations 6 , 7 into $v_k(K)$.

$$v_k(K) = \begin{bmatrix} e^{-jK^T P_0} \\ e^{-jK^T P1} \\ \vdots \\ . \\ . \\ e^{-jK^T P_{N-1}} \end{bmatrix} \tag{8}$$

$$v_k(k_z) = \left[e^{j\left(\frac{N-1}{2}\right)k_z d} \middle| e^{j\left(\frac{N-1}{2}-1\right)k_z d} \middle| \dots \dots \middle| e^{j\left(\frac{N-1}{2}-1\right)k_z d} \right]^T \tag{9}$$

Through;

$$k_z = -\frac{2\pi}{\lambda} cos\theta = -k_0 cos\theta \tag{10}$$

Where k_0 represents the magnitude of the signal wavenumber.

$$k_0 \triangleq |k| \triangleq \frac{2\pi}{\lambda} \tag{11}$$

Note that for the uniform linear array antenna has no resolution capability in the ϕ-direction. Substituting complex weight vector $W^H = [w_0^* \ w_1^* \ \dots \ w_{N-1}^*]$ and $v_k(k)$ into $\gamma(\omega, k) = W^H v_k(k)$ gives the following equation;

$$\gamma(\omega, k_z) = w^H v_k(k_z) = \sum_{n=0}^{N-1} \omega_n^* e^{-j\left(n - \frac{N-1}{2}\right) k_z d} \tag{12}$$

Defining for our convenient;

$$\psi = -k_z d = \frac{2\pi}{\lambda} cos\theta . d = \frac{2\pi}{\lambda} u_z d \tag{13}$$

where $u_z = cos\theta$ is the cosine direction around the z-axis. $\gamma_\psi(\psi)$ can be computed with the help of Equations 12 and 13 which gives.

$$\gamma_\psi(\psi) = e^{-j\frac{N-1}{2}\psi} \sum_{n=0}^{\hat{}} \omega_n^* e^{jn\psi} \tag{14}$$

Frequency wavenumber function in ψ- space is represented by $\gamma_\psi(\psi)$.

Table 4. Visible region of $\gamma(\omega, k_z)$ and $\gamma_\psi(\psi)$ with respect to Frequency Wavenumber Function.

Frequency Wavenumber Function	$\gamma(\omega, k_z)$	$\gamma_\psi(\psi)$
Range	$-\infty\ to\ \infty$	$-\infty\ to\ \infty$
Propagation Signal Region in terms of θ	$0 \le \theta \le \pi$	$0 \le \theta \le \pi$
Propagation Signal Region in terms of u_z	$-1 \le u_z \le 1$	$-1 \le u_z \le 1$
Restriction implies in terms of ψ	$-\frac{2\pi d}{\lambda} \le \psi \le \frac{2\pi d}{\lambda}$	$-\frac{2\pi d}{\lambda} \le \psi \le \frac{2\pi d}{\lambda}$
Restriction implies in terms of k_z	$-\frac{2\pi}{\lambda} \le k_z \le \frac{2\pi}{\lambda}$	$-\frac{2\pi}{\lambda} \le k_z \le \frac{2\pi}{\lambda}$

Visible region of $\gamma(\omega, k_z)$ and $\gamma_\psi(\psi)$ with respect to Frequency Wavenumber Function is represented in Table 4. The beam patterns can be written in three different formats represented in Table 5. The key difference between the frequency wavenumber and the beam pattern is that the beam pattern parameters are limited to correspond to the physical angle θ.

Table 5. Three Different Format of Beampattern.

Beam Pattern	Mathematical Expression	Range of Beam Pattern
$B_\theta(\theta) = w^H v_\theta(\theta)$	$e^{-j\left(\frac{N-1}{2}\right)\frac{2\pi d}{\lambda}cos\theta \sum_{n=0}^{N-1} \omega_n^* e^{jn\frac{2\pi d}{\lambda}cos\theta}}$	$0 \le \theta \le \pi$
$B_u(u) = w^H v_u(u)$	$e^{-j\left(\frac{N-1}{2}\right)\frac{2\pi d}{\lambda}u \sum_{n=0}^{N-1} \omega_n^* e^{jn\frac{2\pi d}{\lambda}u}}$	$-1 \le u \le u$
$B_\psi(\psi) = w^H v_\psi(\psi)$	$e^{-j\left(\frac{N-1}{2}\right)\frac{2\pi d}{\lambda}\psi \sum_{n=0}^{N-1} \omega_n^* e^{jn\psi}}$	$-\frac{2\pi d}{\lambda} \le \psi \le \frac{2\pi d}{\lambda}$

Suppose $B_\psi(\psi) = w^H v_\psi(\psi)$ is defined in Table 5. In other words, it is generated from the complex Nx1 vector w. If you start with, use an arbitrary function $B_\psi(\psi)$ and $w = [V^H\psi]^{-1}B^H$ to generate a pattern that matches $B(\psi_i), i = 1, \dots N$ but does not necessarily match function $B_\psi(\psi)$. We present this result in the context of a uniform linear array. However, the derivation is valid for any N-element array geometry.

2-3- The Smart City Scenario of a 5G Smart Devices for Machine-to-Machine Talk Integration

Considering the coordinates system of smart devices layout of the system antenna array for the smart city scenario of a 5G smart devices for Machine-to-Machine talk integration as defined in Lau et al. (2000) [22]. A longer smart devices is along the y-axis, and a smaller smart devices is along the x-axis. The ULA antenna array can be placed along the z-axis. If the smart device antenna array is bent, the displacement is on the z-axis. Flexible electronics smart devices often have a wraparound provision. In this case, the array is still in the yz-plane, but curved downward in the negative direction z-axis. As before, the first and last elements of the curved array are not on the y-axis.

3- Matlab Based Simulation Methodology of MRLAs and ULAs Model

This section describes the simulation methods of proposed MRLAs and ULAs Model. The simulation is performed in MATLAB. Considering the current form factor of 6 inches of smart electronics devices with operating frequency of 30 GHz, the ULA size is fixed at 7 elements. Antenna elements are not customized, and elemental patterns do not appear in the analysis because they correspond to a specific type. The far-field mode depends only on the array and can be mathematically analyzed and evaluated.

3-1- Array Factor Calculation

The first term is often referred to as the beam pattern of an array with isotropic elements. MRLA structure of Figure 2 need to be converted to the ω_n format. For example, for a four-element MRLA, the value of ω_n is {0 1 4 6} and an aperture of {1 1 0 0 1 0 1} can be provided. Conveniently represented as an array factor as follows:

$$AF(k_z) = \triangleq \sum_{n=0}^{N-1} \omega_n^* . e^{-jk_z z_n} \tag{15}$$

The steps followed to evaluate the antenna array response of a flexible or curved array is shown in Figure 4.

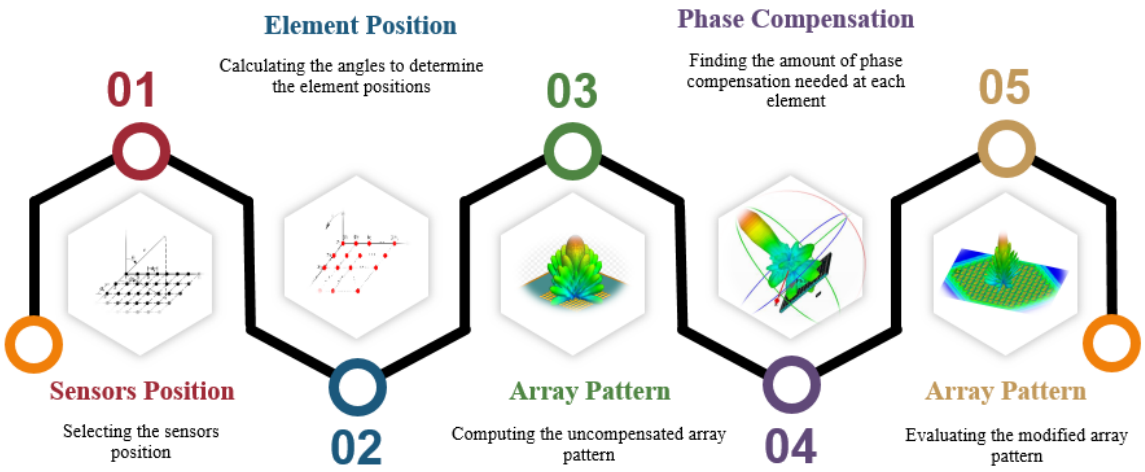

Figure 4. Steps to evaluate the antenna array response of a flexible or curved array.

A total number of 132 MRLA configurations can provide for the required $N = 4, N_a$ = 6 openings. All possible configurations of MRLAs for $N = 3 \rightarrow 17$ is summarized in Table 3.

4- Experimental Results and Analysis

Consider a standard linear array with 7 elements of weighting for $\psi_0 = 0.1\pi, 0.2\pi, 0.3\pi, 0.\pi 4$. Figure 5 illustrates the Beam patterns as a function of $\psi_0 = 0.1\pi, 0.2\pi, 0.3\pi, 0.\pi 4$, Discrete Prolate Spheroidal Sequences (DPSS) weighting, N=7. Computer simulated $HPBW\left(u = \frac{\psi}{\pi}\right)$, $HPBW(deg)$, $BW_{NN}\left(u = \frac{\psi}{\pi}\right)$, $BW_{NN}(deg)$ and the height of highest sidelobe (SL Ht.(dB)) is shown in Table 6.

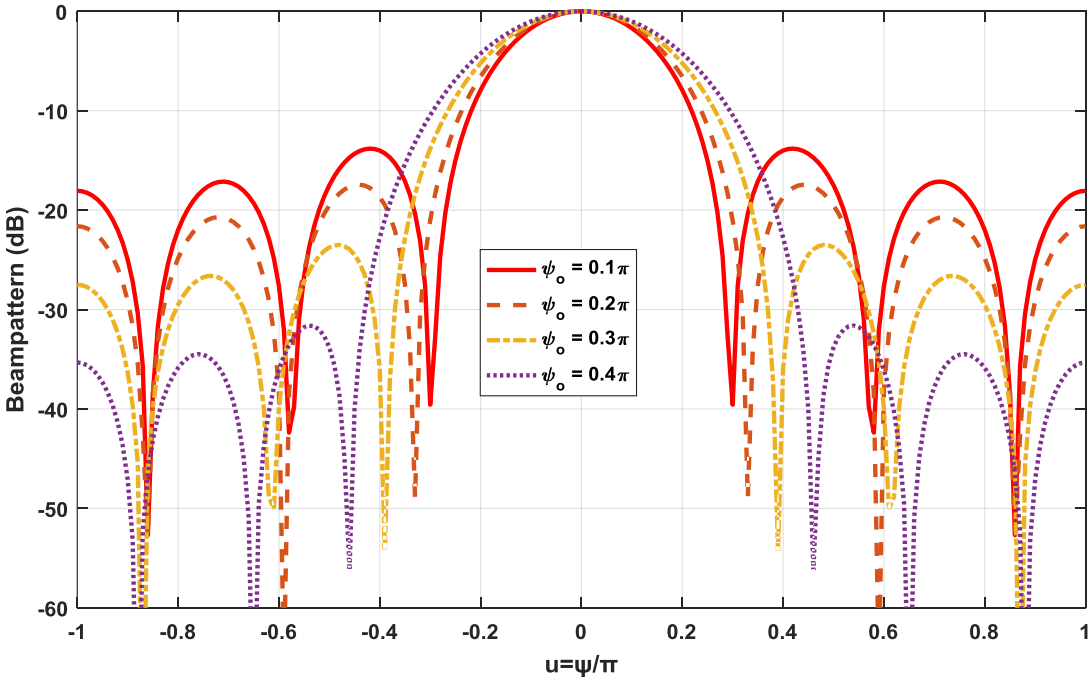

Figure 5. Beam patterns as a function of $\psi_0 = 0.1\pi, 0.2\pi, 0.3\pi, 0.\pi 4$: Discrete Prolate Spheroidal Sequences (DPSS) weighting, N=7.

Consider 4-element array equivalent to a standard linear array with a 7-element aperture of ideal MRLA shown in Figure 2 with $d = \lambda/2$. Figure 6 shows a beam pattern with uniform weights. HPBW is 0.666 and is BWNOT is 1.385 in ψ-spaces. The beampattern does not have true nulls $(B(\psi) = 0)$, therefore the "null-to-null beamwidth is really the " minimum-to minimum" beamwidth. The minima occur at $\psi_m = \pm 0.2205\pi = \pm 0.6927$ with $B(\psi_m) = 0.0862$. Thus $BW_{mm} = 0.4410\pi = 1.3854$.

i. For 7-element uniform linear array, null occur at $\psi_N = \pm\frac{2}{7} = 0.0910\pi = 0.2858$, with $BW_{NN} = \frac{4}{7} = 0.5714\pi = 1.7952$.

ii. 4-element array has narrower mean beam.
iii. 4-element array has much higher sidelobes and shallow nulls.

We use a BW notch-notch because the beam pattern does not have perfect zeros. In comparison, the standard 4-element arrays are 1.429 and 3.1416, while the standard 7-element linear arrays are 0.801 and 1.795 respectively. Therefore, in terms of main lobe features, MRLA is an improvement over the standard 7-element array.

Table 6. Half Power Beam Width ($HPBW$) and BW_{NN} (null to null) for different Weight.

ψ_0	0.1π	0.2π	0.3π	0.4π
	0.8655	0.5872	0.3542	0.2144
	0.9387	0.7993	0.6569	0.5433
	0.9845	0.9470	0.9044	0.8652
Weight	1.0000	1.0000	1.0000	1.0000
	0.9845	0.9470	0.9044	0.8652
	0.9387	0.7993	0.6569	0.5433
	0.8655	0.5872	0.3542	0.2144
$HPBW\left(u=\frac{\psi}{\pi}\right)$	0.2622	0.2818	0.3100	0.3396
$HPBW(deg)$	15.0663	16.1999	17.8336	19.5524
$BW_{NN}\left(u=\frac{\psi}{\pi}\right)$	0.5934	0.6626	0.7772	0.9238
$BW_{NN}(deg)$	34.5190	38.6954	45.7348	55.0196
SL Ht.(dB)	-13.8148	-17.4409	-23.5034	-33.8102

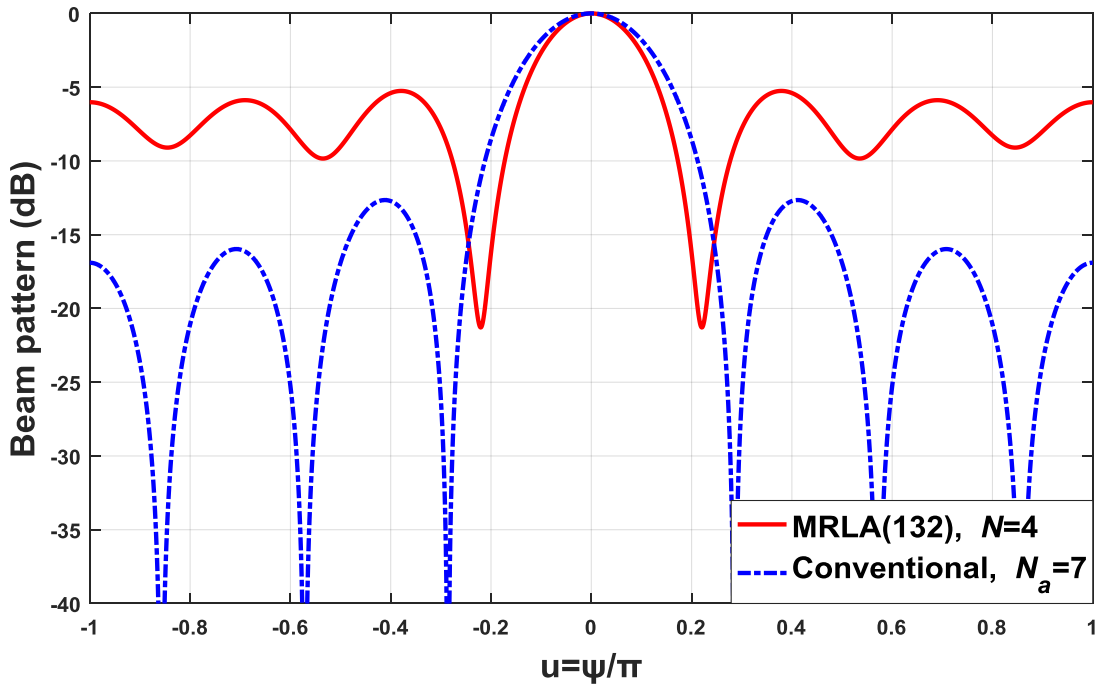

Figure 6. Beam pattern of a uniformly weighted 4-element MRLAs and Conventional (ULAs).

Table 7. Minimum redundancy arrays HPBW, BW and BW_{NN} null-to null for Non-Uniform and Uniform 4 –element arrays.

Specification	Computer Simulated Values
$HPBW$ Non-uniform 4-element array	0.6616
$HPBW$ Uniform 4-element array	1.4307
$HPBW$ Uniform 7-element array	0.8024
BW_{MM} (min-min) Non-uniform 4-element array	1.3854
BW_{NN} (null-null) Uniform 4-element array	1.7957
BW_{NN} (null-null) Uniform 7-element array	1.7957

Table 7 illustrates MRLAs HPBW, BW and BW_{NN} null-to null for non-uniform and uniform 4-element arrays. Consider $N = 5, N_R = 1, N_a = 9$ and case (i) arrays 1332, case (ii) arrays 3411 as per Table 3. Beam pattern for 5-element arrays 1332 MRLAs and conventional (ULAs) is shown in Figure 7 (a).

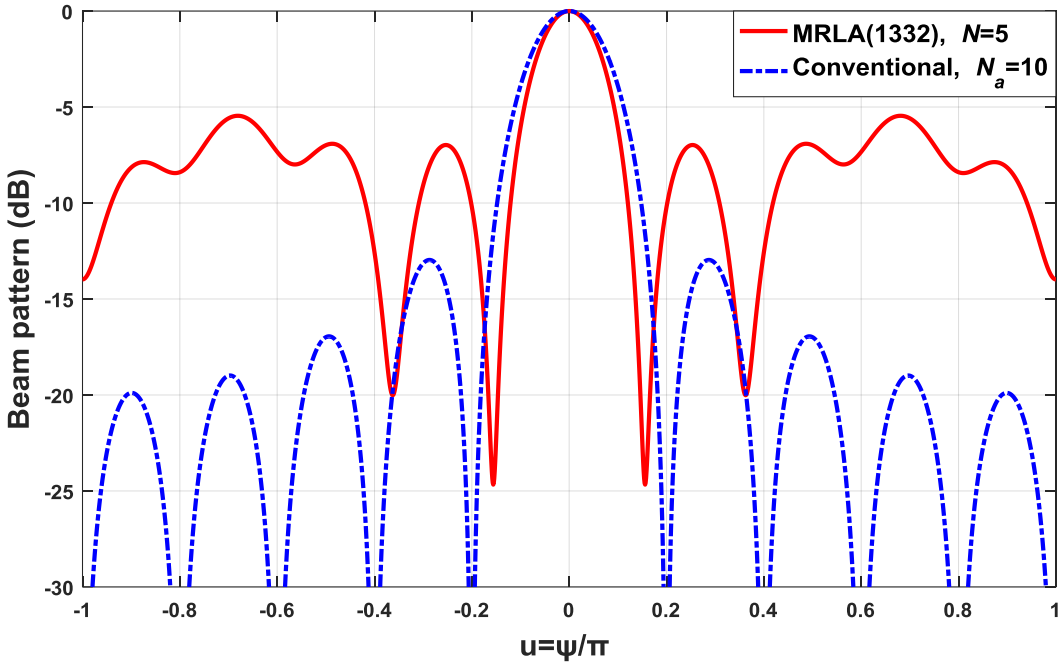

Figure 7 (a). Beam pattern for 5-element arrays 1332 MRLAs and conventional (ULAs).

Table 8. Minimum redundancy arrays HPBW and BW_{NOT} for 5-element array.

Case	HPBW	BW_{NOT}
Case 1 (1,3,3,2)	*0.464*	*0.98*
Case 2 (3,4,1,1),	*0.473*	*0.94*

Beam pattern for 5-element arrays 3411 MRLAs and conventional (ULAs) is shown in Figure 7(b). Table 8 represents minimum redundancy arrays HPBW and BW_{NOT} for 5-element array. In contrast, the standard 10-element linear arrays are 0.559 and 1.25, respectively. As with the uniform linear case, non-uniform weighting can be used to improve sidelobe behavior.

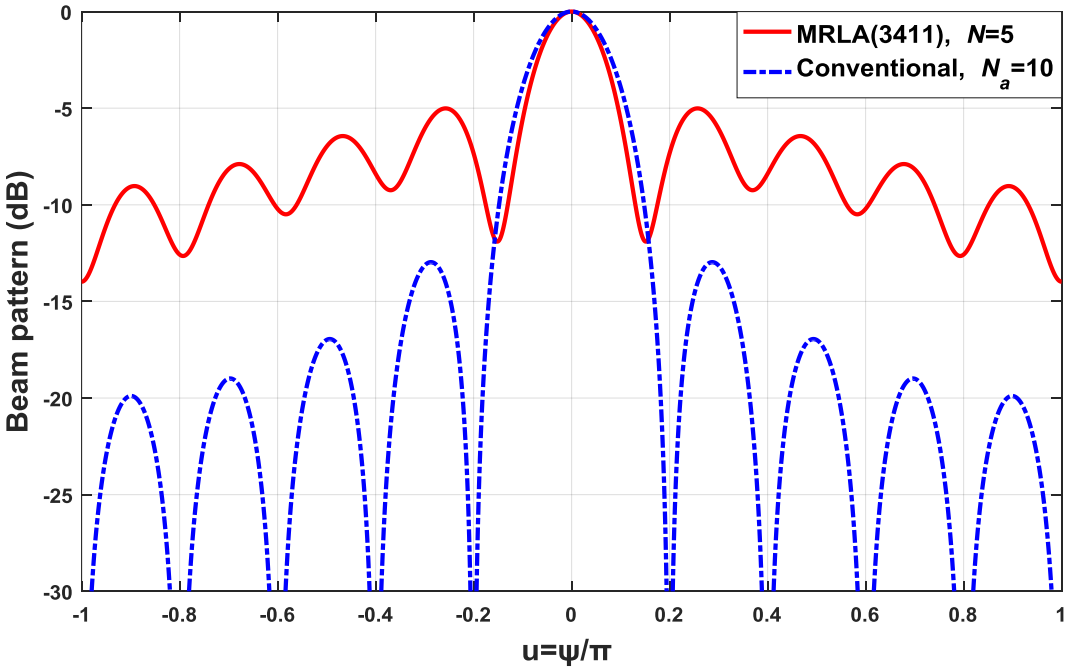

Figure 7 (b). Beam pattern for 5-element arrays 3411 MRLAs and conventional (ULAs).

4-1- MRLA Sidelobe Reduction Algorithms

To reduce the sidelobe in MRLA, develop an algorithm that gives a simple iterative technique for constructing desired beam patterns for arbitrary arrays. The goal is to discover weights that maximize the array's directivity while adhering to a set of beam pattern limitations that limit sidelobe levels. The approach is developed in the setting of linear arrays of isotropic elements, but it can also be used with arrays of any shape and non-isotropic elements. I assume a linear array of isotropic elements with NX1 array response vector $v(u)$ The directivity is indicated by D when the pattern response at the primary response axis or pointing direction is equal to one.

$$D = \left\{\frac{1}{2}\int_{-1}^{1}|B(u)|^2 du\right\}^{-1} \tag{16}$$

$$= \left\{\frac{1}{2}\int_{-1}^{1}|W^H v(u)|^2\, du\right\}^{-1} = \{W^H A W\}^{-1} \tag{17}$$

where:

$$A = \frac{1}{2}\int_{-1}^{1} v(u)v^H(u)du \tag{18}$$

The following are the entries in A:

$$[A]_{mn} = sinc\left(\frac{2\pi}{\lambda}|p_m - p_n|\right)$$

where p_n denotes the nth element's location. Let $V_T = v(u_T)$ be the steering direction's array response vector. The primary difficulty is to maximize directivity (more accurately, decrease the inverse of directivity) while adhering to the unity response constraint on the major response axis.

$$\min w^H A w \;\; s.t\; w^H v_T = 1 \tag{19}$$

The solution for sidelobe reduction is mathematically expressed as follows:

$$w = A^{-1}v_T(v_T^H A^{-1} v_T)^{-1} \tag{20}$$

The maximum directivity weight vector is the uniform weight vector steered in the desired direction, $w = \frac{1}{N}v_T$, in the exceptional situation of a uniform linear array, A = I. For both uniformly and non-uniformly spaced arrays, my aim is to reduce sidelobes by sacrificing some directivity. This can be done by splitting u-space into r sectors (Ω_1, Ω_2, …..Ω_r etc.) and defining a desired (but not necessarily realizable) beam pattern in each sector. Limiting discrepancies between the synthesized and required beam pattern. Assume that $B_{d,i}(u) = w_{d,i}^H v(u)$ represents the equivalent beam pattern. Over region Ω_1, the square error between the beam pattern generated by the synthesized weight vector w and the desired beam pattern is:

$$\epsilon_i^2 = \int\left|B(u) - B_{d,i}(u)\right|^2 du = \int\left|w^H v(u) - w_{d,i}^H v(u)\right|^2 du = \left(w - w_{d,i}\right)^H Q_i\left(w - w_{d,i}\right) \tag{21}$$

where;

$$Q_i = \int v(u)v(u)^H du \tag{22}$$

Considering $\Omega_1$be the region $u_i - \Delta_i$, $u_i + \Delta_i$. The following are the entries in Q_i:

$$[Q_i]_{mn} = e^{j\frac{2\pi}{\lambda}(p_m - p_n)} 2\Delta_i sinc\left(\frac{2\pi\Delta_i}{\lambda}|(p_m - p_n)|\right) \tag{23}$$

Now, subject to pattern error limitations, I can maximize directivity as follows:

$$min \;\; w^H A_w \; s.t\; w^H v_T = 1 \tag{24}$$

s.t $\left(w - w_{d,i}\right)^H Q_i\left(w - w_{d,i}\right) \le L_i \qquad 1 \ldots\ldots r.$

Define:

$$F = w^H A_w + \lambda_0(w^H v_T - 1) + \lambda_0^*(v_T^H w - 1) + \sum_{i=1}^{r}\lambda_i\left(w - w_{d,i}\right)^H Q_i\left(w - w_{d,i}\right) \tag{25}$$

When I differentiate with respect to w^H and setting the result equal to zero, gives expression as follows;

$$A_w + \lambda_0 v_T^H \sum_{i=i}^{r} \lambda_i \left[Q_i (w - w_{d,i}) \right] = 0 \tag{26}$$

A_Q and w_Q are defined as follows:

$$A_Q = A + \sum_{i=1}^{r} \lambda_i Q_i \tag{27}$$

And;

$$w_Q = \sum_{i=1}^{r} \lambda_i Q_i w_{d,i} \tag{28}$$

Eqn. (26) can be written as follows;

$$w = -\lambda_0 + A_Q^{-1} v_T + A_Q^{-1} w_Q \tag{29}$$

Substituting the result of the λ_0 into Equation 29 yields:

$$w = A_Q^{-1} v_T \left(v_T^H A_Q^{-1} v_T \right)^{-1} + \left[A_Q^{-1} - A_Q^{-1} v_T \left(v_T^H A_Q^{-1} v_T \right)^{-1} v_T^H A_Q^{-1} \right] w_Q \tag{30}$$

By establishing a set of small sectors in the sidelobe zone and setting the desired beam pattern to zero in these regions, can achieve tight sidelobe control. In each sector, the desired weight vector is simply the all-zero vector. The pattern error constraints become limits on the magnitude squared of the beam pattern at every location in the sidelobe area in the limit of infinitesimally small sectors. The highest acceptable sidelobe level can be specified as the allowed deviation, and the sidelobe levels can be regulated directly. I can manage sidelobe levels fairly accurately by picking wider but relatively tiny sectors. Further, if I only constrain pattern "error" in the sidelobe region rather than the main beam, the intended weight vector in each constrained sector will be zero, and the second term in Equation 30 will be removed, resulting in a weight vector of zero.

$$w = A_Q^{-1} v_T \left(v_T^H A_Q^{-1} v_T \right)^{-1} \tag{31}$$

To achieve the sidelobe level limitations, an iterative procedure can be employed to change the loading levels. The pattern errors are computed and validated against the restrictions at each iteration. If a constraint is exceeded, the sector's loading is increased, and the weights are adjusted. The iteration steps followed to evaluate the convergence criterion is shown in Figure 8.

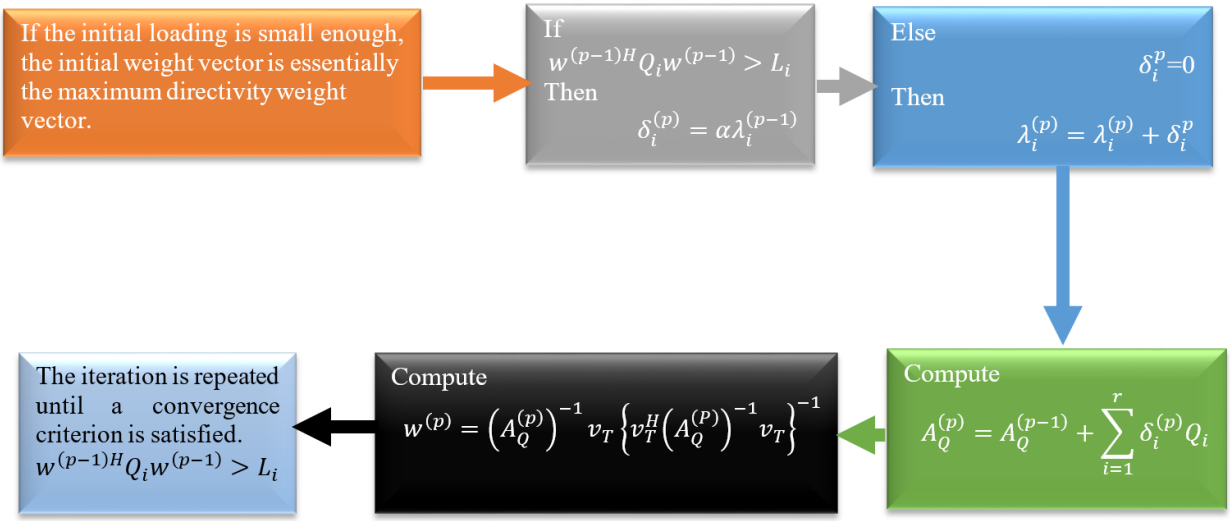

Figure 8. Steps to evaluate the repetitive iteration until conversion criterion satisfied.

The iterative SSL reduction technique is tested for numerous cycles using a conventional 10-element MRLA array, as illustrated in Figure 8. $u_T = 0$ is the ideal look direction, while -30 dB is the desired sidelobe level considered? 80 sidelobe regions are originally established as sectors with a width of $2\Delta_i = 0.02$ in the region $0 \le u \le -0.2$ and $0.2 \le u \le 1$. The constraint levels are all set to $L_i = 2 \times 10^{-5}$, which is the sidelobe level multiplied by the width of each region. $\lambda_0 = 1$ and $\alpha = 0.3$ are the starting loading levels. Figure 9 depicts the progression of the beam pattern and sidelobe region. After 14 repetitions iteration, the final beam pattern is established.

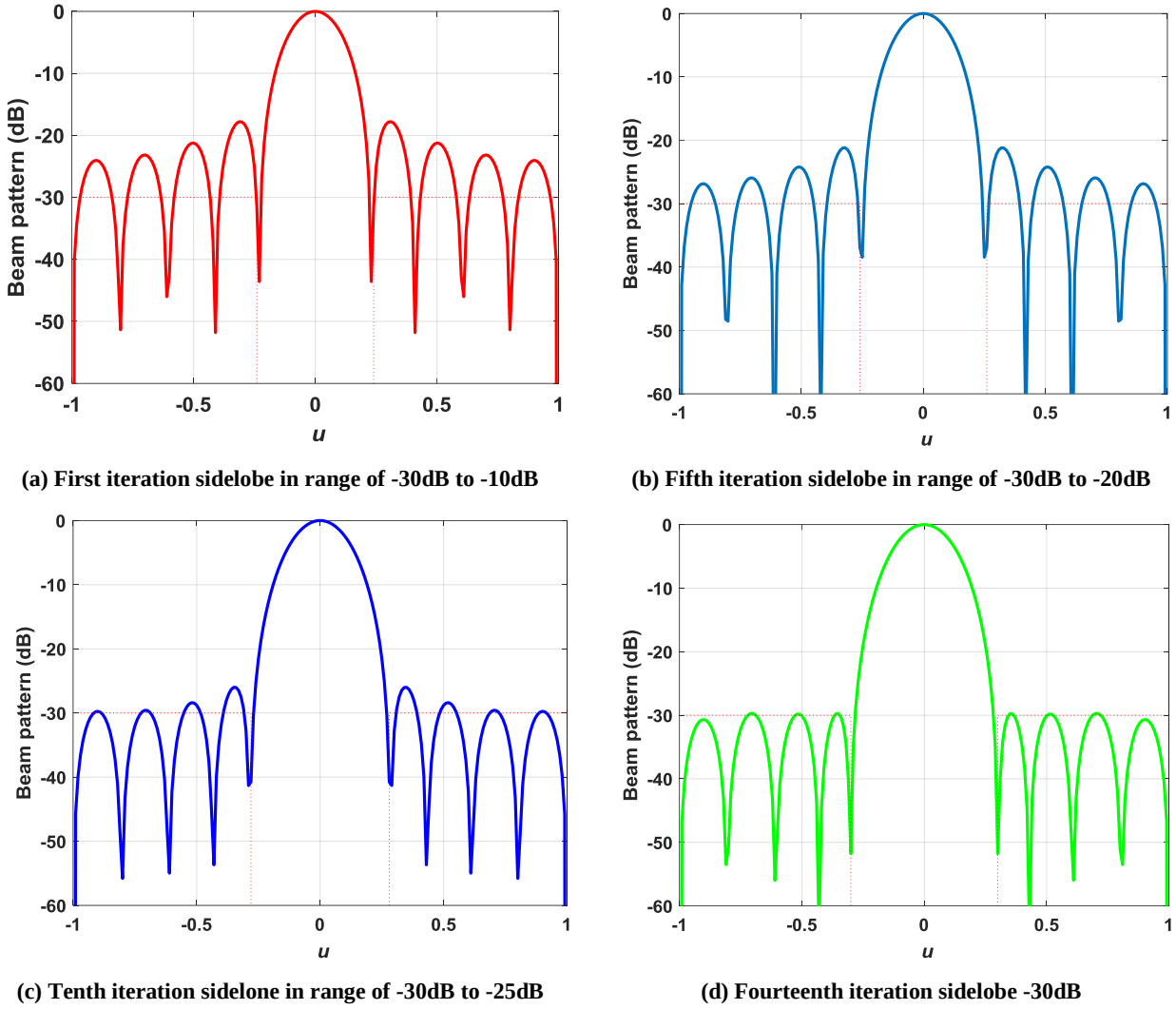

(a) First iteration sidelobe in range of -30dB to -10dB

(b) Fifth iteration sidelobe in range of -30dB to -20dB

(c) Tenth iteration sidelone in range of -30dB to -25dB

(d) Fourteenth iteration sidelobe -30dB

Figure 9. Iteration approaches for SLL -30dB sidelobe reduction.

4-2- Result Comparison with Previous Work

It has been demonstrated that when sensor elements are arranged in the minimum redundancy fashion, an M element array can be made to estimate the directions of arrival of as many as M (M -1)/2 uncorrelated sources unambiguously using an augmentation technique on the covariances obtained from the array outputs [23] First, for uniform spatial sampling with M and N sensors where M and N are co-prime with sufficient interelement spacing, the difference co-array has O (MN) freedoms exploited in beam forming and in the direction of arrival estimation. Their motivation for this array extension scheme is to achieve a co-array difference which fully populated all the lags. It is an interesting question to contrast Vaidyanathan and Pal's proposed single array extension scheme with the ECSA approach proposed in this paper, which extends both subarrays. Their motivation for this array extension scheme is to achieve a co-array difference, which fully populated all the lags. The proposed coprime sensor array (CSA) by Kaushallya Adhikari is a non-uniform linear array obtained by intersection of two uniform linear arrays (ULAs) that are undersampled by coprime factors [24]. A CSA uses fewer sensors to resolve a fully populated ULA of the same aperture. The peak side lobe level in a CSA is however higher than the peak lobe with the same resolution of the comparable maximum ULA side. Adding more sensors to a CSA may reduce the level of its peak side lobe.

5- Conclusion

This study came up with the concept of MRLAs and its advantages for 5-G smart devices application for future Machine-Machine talk integration. Synthesis techniques for MRLAs and ULAs spacing were developed and processing modes result has been compared. Synthesis of low sidelobe differential beams; these beams are widely used in Machine – Machine talk applications to estimate the angle at which the plane wave signal reaches the array from the target has been analyzed. Array construction procedure developed to evaluate the integer position of a particular sensor array over a specified distance, so the missing integer is represented as the difference between the two sensor positions. The main advantage of MRLAs is that it can directly synthesize very large refined arrays with

very low computations and the lowest verbosity ever reported. MRLAs configurations can be used to define a new high-resolution synthetic aperture interferometer array structure for smart devices. The pattern in the center of the array facilitates the construction of space-scalable structures. Experimental results show that MLRAs 4-element array has a narrower mean beam and has much higher sidelobes and shallow nulls. Therefore, in terms of main lobe features, MRLAs has an improvement over the standard 7-element ULAs array.

6- Declarations

6-1- Data Availability Statement

The data presented in this study are available on request from the corresponding author.

6-2- Funding

The authors received no financial support for the research, authorship, and/or publication of this article.

6-3- Conflicts of Interest

The authors declare that there is no conflict of interests regarding the publication of this manuscript. In addition, the ethical issues, including plagiarism, informed consent, misconduct, data fabrication and/or falsification, double publication and/or submission, and redundancies have been completely observed by the authors.

7- References

[1] Marcus, Michael J. "5G and 'IMT for 2020 and Beyond' [Spectrum Policy and Regulatory Issues]." IEEE Wireless Communications 22, no. 4 (August 2015): 2–3. doi:10.1109/mwc.2015.7224717.

[2] Pearson, D., S.U. Pillai, and Y. Lee. "An Algorithm for Near-Optimal Placement of Sensor Elements." IEEE Transactions on Information Theory 36, no. 6 (1990): 1280–1284. doi:10.1109/18.59928.

[3] BouDaher, Elie, Fauzia Ahmad, Moeness G. Amin, and Ahmad Hoorfar. "Mutual Coupling Effect and Compensation in Non-Uniform Arrays for Direction-of-Arrival Estimation." Digital Signal Processing 61 (February 2017): 3–14. doi:10.1016/j.dsp.2016.06.005.

[4] Zhang, Yan-kui, Hai-yun Xu, Da-ming Wang, Bin Ba, and Si-yao Li. "A Novel Designed Sparse Array for Noncircular Sources with High Degree of Freedom." Mathematical Problems in Engineering 2019 (January 29, 2019): 1–10. doi:10.1155/2019/1264715.

[5] Hong, Wei, Zhi Hao Jiang, Chao Yu, Jianyi Zhou, Peng Chen, Zhiqiang Yu, Hui Zhang, et al. "Multibeam Antenna Technologies for 5G Wireless Communications." IEEE Transactions on Antennas and Propagation 65, no. 12 (December 2017): 6231–6249. doi:10.1109/tap.2017.2712819.

[6] Dahri, Muhammad Hashim, Mohd Haizal Jamaluddin, Muhammad Inam Abbasi, and Muhammad Ramlee Kamarudin. "A Review of Wideband Reflectarray Antennas for 5G Communication Systems." IEEE Access 5 (2017): 17803–17815. doi:10.1109/access.2017.2747844.

[7] Zhu, Qian, Kung Bo Ng, Chi Hou Chan, and Kwai-Man Luk. "Substrate-Integrated-Waveguide-Fed Array Antenna Covering 57–71 GHz Band for 5G Applications." IEEE Transactions on Antennas and Propagation 65, no. 12 (December 2017): 6298–6306. doi:10.1109/tap.2017.2723080.

[8] Mao, Chun-Xu, Steven Gao, and Yi Wang. "Broadband High-Gain Beam-Scanning Antenna Array for Millimeter-Wave Applications." IEEE Transactions on Antennas and Propagation 65, no. 9 (September 2017): 4864–4868. doi:10.1109/tap.2017.2724640.

[9] Romanofsky, Robert R. "Advances in Scanning Reflectarray Antennas Based on Ferroelectric Thin-Film Phase Shifters for Deep-Space Communications." Proceedings of the IEEE 95, no. 10 (October 2007): 1968–1975. doi:10.1109/jproc.2007.905065.

[10] Cheng, Yu Jian, Wei Hong, Ke Wu, Zhen Qi Kuai, Chen Yu, Ji Xin Chen, Jian Yi Zhou, and Hong Jun Tang. "Substrate Integrated Waveguide (SIW) Rotman Lens and Its Ka-Band Multibeam Array Antenna Applications." IEEE Transactions on Antennas and Propagation 56, no. 8 (August 2008): 2504–2513. doi:10.1109/tap.2008.927567.

[11] Chen, Peng, Wei Hong, Zhenqi Kuai, Junfeng Xu, Haiming Wang, Jixin Chen, Hongjun Tang, Jianyi Zhou, and Ke Wu. "A Multibeam Antenna Based on Substrate Integrated Waveguide Technology for MIMO Wireless Communications." IEEE Transactions on Antennas and Propagation 57, no. 6 (June 2009): 1813–1821. doi:10.1109/tap.2009.2019868.

[12] Yang, Binqi, Zhiqiang Yu, Yunyang Dong, Jianyi Zhou, and Wei Hong. "Compact Tapered Slot Antenna Array for 5G Millimeter-Wave Massive MIMO Systems." IEEE Transactions on Antennas and Propagation 65, no. 12 (December 2017): 6721–6727. doi:10.1109/tap.2017.2700891.

[13] Ojaroudiparchin, Naser, Ming Shen, Shuai Zhang, and Gert Frolund Pedersen. "A Switchable 3-D-Coverage-Phased Array Antenna Package for 5G Mobile Terminals." IEEE Antennas and Wireless Propagation Letters 15 (2016): 1747–1750. doi:10.1109/lawp.2016.2532607.

[14] Wenyao Zhai, Vahid Miraftab, Morris Repeta, David Wessel, and Wen Tong. "Dual-Band Millimeter-Wave Interleaved Antenna Array Exploiting Low-Cost PCB Technology for High Speed 5G Communication." 2016 IEEE MTT-S International Microwave Symposium (IMS) (May 2016). doi:10.1109/mwsym.2016.7540293.

[15] Jilani, Syeda Fizzah, and Akram Alomainy. "A Multiband Millimeter-Wave 2-D Array Based on Enhanced Franklin Antenna for 5G Wireless Systems." IEEE Antennas and Wireless Propagation Letters 16 (2017): 2983–2986. doi:10.1109/lawp.2017.2756560.

[16] Ishiguro, Masato. "Minimum Redundancy Linear Arrays for a Large Number of Antennas." Radio Science 15, no. 6 (November 1980): 1163–1170. doi:10.1029/rs015i006p01163.

[17] Hong, Wonbin, Kwang-Hyun Baek, and Seungtae Ko. "Millimeter-Wave 5G Antennas for Smartphones: Overview and Experimental Demonstration." IEEE Transactions on Antennas and Propagation 65, no. 12 (December 2017): 6250–6261. doi:10.1109/tap.2017.2740963.

[18] Ebrahimi, Mohammad, Mahmoud Modarres-Hashemi, and Ehsan Yazdian. "An Efficient Method for Sparse Linear Array Sensor Placement to Achieve Maximum Degrees of Freedom." IEEE Sensors Journal 21, no. 18 (September 15, 2021): 20788–20795. doi:10.1109/jsen.2021.3093889.

[19] Albagory, Yasser. "Direction-Independent and Self-Reconfigurable Spherical-Cap Antenna Array Beamforming Technique for Massive 3D MIMO Systems." Wireless Networks 26, no. 8 (July 20, 2020): 6111–6123. doi:10.1007/s11276-020-02434-9.

[20] Juárez, Elizvan, Marco A. Panduro, Alberto Reyna, David H. Covarrubias, Aldo Mendez, and Eduardo Murillo. "Design of Concentric Ring Antenna Arrays Based on Subarrays to Simplify the Feeding System." Symmetry 12, no. 6 (June 8, 2020): 970. doi:10.3390/sym12060970.

[21] Chakravarthy, V. V. S. S. S., and P. Mallikarjuna Rao. "Circular array antenna optimization with scanned and unscanned beams using novel particle swarm optimization." Indian Journal of Applied Research 5, no. 4 (2015).

[22] Lau, B.K., and Y.H. Leung. "A Dolph-Chebyshev Approach to the Synthesis of Array Patterns for Uniform Circular Arrays." 2000 IEEE International Symposium on Circuits and Systems. Emerging Technologies for the 21st Century. Proceedings (IEEE Cat No.00CH36353) (May 2000). doi:10.1109/iscas.2000.857042.

[23] Pearson, D., S.U. Pillai, and Y. Lee. "An Algorithm for Near-Optimal Placement of Sensor Elements." IEEE Transactions on Information Theory 36, no. 6 (1990): 1280–1284. doi:10.1109/18.59928.

[24] Ruf, C.S. "Numerical Annealing of Low-Redundancy Linear Arrays." IEEE Transactions on Antennas and Propagation 41, no. 1 (1993): 85–90. doi:10.1109/8.210119.

[25] Linebarger, D.A., I.H. Sudborough, and I.G. Tollis. "Difference Bases and Sparse Sensor Arrays." IEEE Transactions on Information Theory 39, no. 2 (March 1993): 716–721. doi:10.1109/18.212309.

[26] Linebarger, D.A. "A Fast Method for Computing the Coarray of Sparse Linear Arrays." IEEE Transactions on Antennas and Propagation 40, no. 9 (1992): 1109–1112. doi:10.1109/8.166540.

[27] Hong, Wonbin, Kwang-Hyun Baek, and Seungtae Ko. "Millimeter-Wave 5G Antennas for Smartphones: Overview and Experimental Demonstration." IEEE Transactions on Antennas and Propagation 65, no. 12 (December 2017): 6250–6261. doi:10.1109/tap.2017.2740963.

[28] Vaidyanathan, Palghat P., and Piya Pal. "Sparse Sensing With Co-Prime Samplers and Arrays." IEEE Transactions on Signal Processing 59, no. 2 (February 2011): 573–586. doi:10.1109/tsp.2010.2089682.

[29] Adhikari, Kaushallya, John R. Buck, and Kathleen E. Wage. "Extending Coprime Sensor Arrays to Achieve the Peak Side Lobe Height of a Full Uniform Linear Array." EURASIP Journal on Advances in Signal Processing 2014, no. 1 (September 27, 2014). doi:10.1186/1687-6180-2014-148.